Energy Conversion and Management 52 (2011) 2170–2182

Contents lists available at ScienceDirect

Energy Conversion and Management

journal homepage: www.elsevier.com/locate/enconman

Heat transfer from a permeable square cylinder to a flowing fluid

S. Dhinakaran [a,*], J. Ponmozhi [b,1]

[a] CEFT, Departamento de Engenharia Química, Faculdade de Engenharia da Universidade do Porto, Rua do Doutor Roberto Frias, 4200 465 Porto, Portugal
[b] Departamento de Engenharia Mecânica, Universidade de Aveiro, Campus Universitario de Santiago, 3810 193 Aveiro, Portugal

ARTICLE INFO

Article history:
Received 25 January 2010
Received in revised form 29 November 2010
Accepted 31 December 2010

Keywords:
Permeable square cylinder
Heat transfer enhancement
Forced convection
Single-domain approach
Brinkman model

ABSTRACT

Flow and heat transfer from an isolated square cylinder maintained at a constant temperature is considered. The cylinder is porous with constant permeability and porosity. The cylinder is placed horizontally and is subjected to an uniform flow of air. Forced convection heat transfer from the cylinder is analyzed for different values of Darcy numbers (10^{-6}–10^{-2}) at low Reynolds numbers. Brinkman model with an additional Forchheimer term has been used to model the flow in the porous media. The effect of Darcy number and porosity on the drag coefficient, length of the wake behind the cylinder, Nusselt number at each face of the cylinder and the overall Nusselt number of the cylinder have been analyzed for Reynolds numbers 1–40.

The important results of the study can be summarised as follows:

- The flow is steady for the range of Reynolds and Darcy numbers considered here. The flow pattern through and around the porous cylinder depends much on the Darcy number of the porous medium. At small Darcy numbers (=10^{-6}), the permeable cylinder behaves like a solid cylinder with no fluid penetrating the surface. With increasing Darcy numbers the fluid starts penetrating the surface with ease.
- The drag coefficient, mean Nusselt number and wake length of the permeable square cylinder approaches the corresponding case of a impermeable cylinder placed in an unbounded domain for very low Darcy number, typically at Darcy numbers 10^{-6}. With increasing Darcy number the drag coefficient and wake length decreases. Flow separation from the cylinder is delayed with increasing Darcy number.
- Fluid impinging the front surface carries away more heat than any other surface resulting in a high local Nusselt number along the front surface which increases with increase in Darcy number while it decreases along the other three faces. But the mean Nusselt number of the cylinder shows an enhancement in heat transfer rates with increasing Darcy numbers and Reynolds number.

1. Introduction

Owing to its fundamental and practical importance a significant research effort has been expended in studying the flow past a square cylinder immersed in a fluid stream. Flow past buildings, bridges, electronic components, etc., are akin to flow around square cylinders and is thus important to analyze the flow and heat transfer characteristics of this configuration. Although the shape of this body is simple, it offers rich fluid mechanics features of flow separation, wake formation, vortex shedding, etc. Moreover, a reliable knowledge of engineering parameters such as drag coefficient, wake size, and Nusselt number, are required for the design of structures such as cooling towers, antennas, heat exchangers and electronic devices. Depending on the Reynolds number, the flow past a square cylinder exhibits fully-attached flow regimes ($Re \leqslant 2$), twin attached vortex flow regime ($2 > Re \leqslant 40$) and laminar vortex shedding flow regimes ($Re > 40$). Works on flow and heat transfer from square cylinders are abundant in the literature. Franke et al. [1] studied the laminar flow past a square as well as a circular cylinder at low Reynolds numbers. Their calculation showed a steady flow at Reynolds number 40 for the circular as well as the square cylinder. Zaki et al. [2] numerically and experimentally investigated the flow past a square cylinder at low and high Reynolds numbers, respectively. The drag coefficient, lift coefficient, surface pressure and mean wake length formed behind a square cylinder was numerically studied by Sohankar et al. [3] for Reynolds numbers in the range 45–250. The flow pattern showed an alternate row of vortices shed from the cylinder called

* Corresponding author. Tel.: +351 225 08 1779; fax: +351 225 081 404.
E-mail addresses: dhina@fe.up.pt, ssdhinakar@gmail.com (S. Dhinakaran), jponmozhi@inegi.up.pt, jponmozhi@gmail.com (J. Ponmozhi).
[1] Present address: Instituto de Engenharia Mecânica e Gestacão Industrial (INEGI), Campus da FEUP, Universidade do Porto, Rua do Doutor Roberto Frias, 4200 465 Porto, Portugal.

0196-8904/$ - see front matter © 2011 Elsevier Ltd. All rights reserved.
doi:10.1016/j.enconman.2010.12.027

Nomenclature

$C1$, $C2$	binary constants
C_p	specific heat capacity
C_D	coefficient of drag
C_{DP}	coefficient of drag due to pressure forces
C_{DV}	coefficient of drag due to viscous forces
Da	Darcy number, $\frac{\kappa}{W^2}$
d	diameter of a particle (m)
F	inertial factor
F_D	drag force (N m^{-2})
k	thermal conductivity (W m^{-1} K^{-1})
L_d	distance between rear face of the cylinder and the outflow boundary (m)
Nu	local Nusselt number, $-R_k \frac{\partial\theta}{\partial n}$
p	dimensional pressure (N m^{-2})
P	dimensionless pressure, $\frac{p^*}{\rho_f U_L^2}$
Pr	Prandtl number, $\frac{\nu}{\alpha}$
Re	Reynolds number, $\frac{U_\infty W}{\nu}$
R_k	ratio of thermal conductivity of porous and fluid layers, $\frac{k_e}{k_f}$
t	dimensional time
T	dimensional temperature (°C)
u, v	x, y-component of velocity (m s^{-1})
U, V	non-dimensional x, y-component of velocity
x, y	horizontal, vertical distance (m)
X, Y	dimensionless horizontal, vertical coordinate
W	height of the cylinder

Greek

ϵ	porosity
δ	smallest grid size
Δ	largest grid size
κ	permeability of the material (m^2)
Λ	viscosity ratio, $\frac{\mu_e}{\mu}$
θ	dimensionless temperature, $\frac{(T-T_\infty)}{(T_w-T_\infty)}$
μ	dynamic viscosity (kg m^{-1} s^{-1})
τ	non-dimensional time, $\frac{tU_\infty}{W}$ (s)
ρ	density

Subscripts

∞	far field value
e	effective value
f	front face
r	rear face
t	top face
b	bottom face
p	particle
w	wall
M	mean value

the 'von Karman Vortex Street'. Sharma and Eswaran [4] analyzed the forced convection heat transfer from a square cylinder, maintained at constant temperature and uniform heat flux, in a uniform flow of air for Reynolds numbers 1–160. The average Nusselt number of the cylinder increased monotonically with increasing Reynolds number. The Nusselt number from the front surface of the cylinder was highest while the rear surface recorded smaller values. For steady flow, the wake length increased almost linearly with increase in Reynolds number while the drag coefficient decreased. Dhiman et al. [5] investigated the effect of Prandtl number on the heat transfer characteristics of a square cylinder in uniform flow for $1 \leqslant Re \leqslant 45$ and $0.7 \leqslant Pr \leqslant 4000$. A monotonic increase in Nusselt number with increase in Reynolds number or Prandtl number was observed in their study. However, these studies dealt with a impermeable/solid square cylinder.

Investigation of flow and heat transfer from permeable bodies (such as porous inserts, blocks, fins, and baffles) is important since they have large contact surface and thus tend to enhance the heat transfer rates compared to their solid counterparts. Several studies were made in this direction to study their flow and heat transfer characteristics. Fu et al. [6] numerically investigated the thermal performance of a single copper porous block mounted on a heated plate in a horizontal channel in laminar flow. The results for the heat transfer rates showed that a porous block can considerably increase the Nusselt number when mounted on a high temperature region compared to the case without a porous block. Guerroudj and Kahalerras [7] analysed the mixed convection heat transfer in a channel with porous blocks of shapes varying from rectangular to triangular, placed on a partially heated lower plate. They found a global increase in Nusselt number at small permeability and for the triangular shape. The triangular shape of the porous block showed highest heat transfer rates at small values of Darcy numbers, Reynolds number and thermal conductivity ratio. The rectangular shape produced an optimum value for higher values of the same parameters. Targui and Kahalerras [8] made a numerical analysis of the heat transfer performance of porous structures placed inside the walls in an annular gap of a counter flow double pipe heat exchanger. They analysed the effect of Darcy number, thermal conductivity ratio, spacing and thickness of porous structures on the heat transfer performance. They found that these porous structures destabilized the flow resulting in recirculation zones that contributed to heat transfer enhancement between the wall and the cold fluid. Heat transfer analysis on the flow in a backward facing step with a porous floor segment was done by Abu-Hijleh [9]. The study indicated that the addition of a porous segment resulted in a reduction in the overall Nusselt number and an increase in the maximum Nusselt number compared to the case of a solid floor. Most of these studies concentrated on the flow and heat transfer characteristics of single or multiple porous objects placed on the walls or plates of channels, or annular regions.

Looking into these studies, it is very clear that heat transfer rates are enhanced with the use of porous materials. With this idea in mind, we propose to study the effect of using an isolated porous square cylinder in a uniform flow of air and compare the obtained results with those of a solid square cylinder. The flow around an isolated permeable body finds application in nuclear biological filters used in pharmaceutical, medical and chemical industries while the heat transfer aspects of the same configuration finds application in LED backlight module cooling system, heat exchangers, nuclear reactors, drying processes, etc., and is also of high academic interest.

1.1. Previous work

Although several articles are available on the flow past an impermeable square cylinder, for both steady and unsteady flow, only a few works are available in the literature concerning the permeable case. Jue [10] numerically investigated the problem of vortex shedding from a porous square cylinder for Reynolds number 100, 200 and 250. Using the single-domain approach and a harmonic-mean formulation at the interface of the porous and fluid layers, he studied the dependence of porosity and Darcy number on the drag coefficient, Strouhal number and flow pattern in and around the cylinder. The computed results indicated an earlier occurence of vortex shedding at lower permeability. A reduction in drag coefficient with increasing value of Darcy number was reported in their study. The computed results for the lift and drag

coefficients did not show any significant difference for variation in porosity compared to the variation in Darcy number. Thus, the flow characteristics depended much on the Darcy number and Reynolds number. Chen et al. [11] numerically investigated the steady and unsteady flow past a porous square cylinder for Reynolds numbers 20, 40, 100 and 200. Using the stress-jump boundary condition of Ochoa-Tapia and Whitaker [12], at the interface of the fluid and porous layers, they analyzed the effect of stress jump parameters at various Darcy numbers and porosity for those Reynolds numbers. For the steady flow, they found that the recirculation region behind the cylinder disappeared for Darcy number greater than 10^{-2}. With a decrease in Darcy number, the recirculation region was clearly seen. The drag coefficient of the cylinder started to decrease with an increase in Darcy number. For the unsteady case, the vortex shedding phenomenon was delayed with increasing Darcy number. Utilizing the Boltzmann model, Babu and Narasimhan [13] studied the effect of a porous square cylinder, placed in a infinite stream, on the wake structure and vortex shedding frequency at $Re = 100$. They varied the Darcy number and Porosity from 0.0001 to 0.1 and 0.25 to 0.9, respectively, and studied the unsteady flow field behind the cylinder. Quantities such as Strouhal number were calculated and compared with those of corresponding solid cylinder to bring out the effect of porous medium. A reduction in vortex shedding with increasing porous medium permeability was observed in their study.

More recently, Yu et al. [14] analysed the flow structure around a square cylinder using the stress-jump boundary condition. They presented the flow structure around the permeable square cylinder, with the help of streamlines, for Reynolds numbers 1–50, Darcy numbers 10^{-6}–10^{-1} and porosity 0.6–0.95. For the range of Reynolds numbers considered in their study the fluid was found to penetrate the cylinder more easily with increasing Darcy number. For certain values of Darcy number, the recirculating eddy behind the cylinder detaches from rear surface and vanishes with an increase in Darcy number. They presented plots of the coordinates of wake centre as a function of Reynolds number for different Darcy number along with the length of the wake formed behind the porous cylinder. The drag coefficient of the permeable square cylinder, which is an important parameter to be considered, was not presented in their study. From the above discussion, it is evident that all these studies concentrated only on the fluid flow characteristics of a porous square cylinder in the steady/unsteady flow regime.

An inspection of the available literature clearly shows that the flow characteristics have been studied, although not so extensively, for the unsteady vortex shedding case than the case of steady flow. But a study of heat transfer from a square permeable cylinder in uniform flow does not exist in the literature. The only study dealing with the heat transfer from a permeable square cylinder is that of Wu and Wang [15,16]. However, the permeable cylinder considered in both these studies were confined in a channel. Wu and Wang [15] analyzed the convective heat transfer performance of a porous square cylinder placed symmetrically in a channel with a constant heat flux being applied only at the bottom surface of the porous cylinder. They studied the heat transfer characteristics for Reynolds in the range 100–700, Darcy numbers in the range 10^{-6}–10^{-2} and porosity in the range 0.4–0.8. Their analysis indicated that the mean Nusselt number was enhanced by 101.70% at Darcy number equal to 0.01 compared to an enhancement of only 0.12% at Darcy number 10^{-6}. More recently, the same authors [16] extended their work for the mixed convection heat transfer in a channel for different channel-to-cylinder gap ratios for Richardson numbers in the range 0–20 and for Darcy numbers 10^{-5}–10^{-2} at a fixed Reynolds number of 250. They found that heat transfer rates increased with increasing channel-to-cylinder height ratio and Darcy number. They showed that by increasing the Richardson number and Darcy number, one could achieve higher heat transfer rates. For example, at Richardson number 20 they got an enhancement of 150.28% at Darcy number 10^{-2} while the enhancement was only 26.91% at Darcy number 10^{-4}.

1.2. Objective of this study

A review of the available literature shows that a study on the forced convection heat transfer from an isolated permeable square cylinder in the laminar steady flow regime has not been made yet although studies dealing with heat transfer from a solid square cylinder exist. Besides, there is no result available in the literature on the drag coefficient of the porous square cylinder which is an important parameter to be considered. The objective of the present work is, therefore, to elucidate in detail the flow and thermal field around an isolated permeable square cylinder and to explore the link between permeability and heat transfer.

Fluid flow in porous media has been historically modeled by Darcy's law [17,18]. The linear nature of the Darcy's law and the fact that it neglects viscous effects near boundaries makes it inadequate for modeling in a variety of different problems. For this reason, a number of extensions have been applied to Darcy's law in the past, including Brinkman's equation [19,20] which incorporates viscous effects, and the Forchheimer equation which incorporates nonlinear drag effects at higher fluid velocities. In case of a composite system consisting of a fluid and porous medium, the governing equations for the fluid and porous regions are combined by one set of conservation equations to model the whole fluid/porous composite system as a single domain governed by one set of conservations, the solution of which satisfies the matching conditions at both fluid/porous interfaces. In this study, we have adapted the single-domain approach [21].

2. Mathematical formulation

2.1. Problem description

The problem under study is shown in Fig. 1a. A fixed 2D square cylinder of height, W, maintained at a constant temperature, T_w, is exposed to a constant free stream velocity U_∞ (flowing in the positive x-direction) which is at an ambient temperature T_∞. The permeable cylinder is exchanging heat with the surrounding fluid. Artificial boundaries are placed at sufficient distance far away from the cylinder in order to make the problem computationally feasible.

2.2. Governing equations

The Brinkman model with an additional Forchheimer term and the Navier–Stokes equations are used to express the flow inside and outside the permeable square cylinder, respectively. A single-domain approach [21] is adopted where a single set of equations are utilized to describe the flow in both the porous and fluid region. The fluid velocity averaged to a volume containing fluid only $(\vec{V})$ and the filter velocity $\vec{v}$ (average of fluid velocity over an elementary volume of solid matrix plus fluid) are related to each other by the Dupuit–Forchheimer equation [17] by $\vec{v} = \epsilon \cdot (\vec{V})$. To simplify the problem the following assumptions are made:

- The porous cylinder is isotropic, homogenous and saturated with a single-phase fluid. The porosity and permeability of the cylinder are uniform.
- The flow is steady, laminar, two-dimensional and incompressible. The effective viscosity of the porous medium and the fluid viscosity are equal.
- There is no internal heat generation in the porous cylinder and viscous dissipation is negligible. Further, the effective conduc-

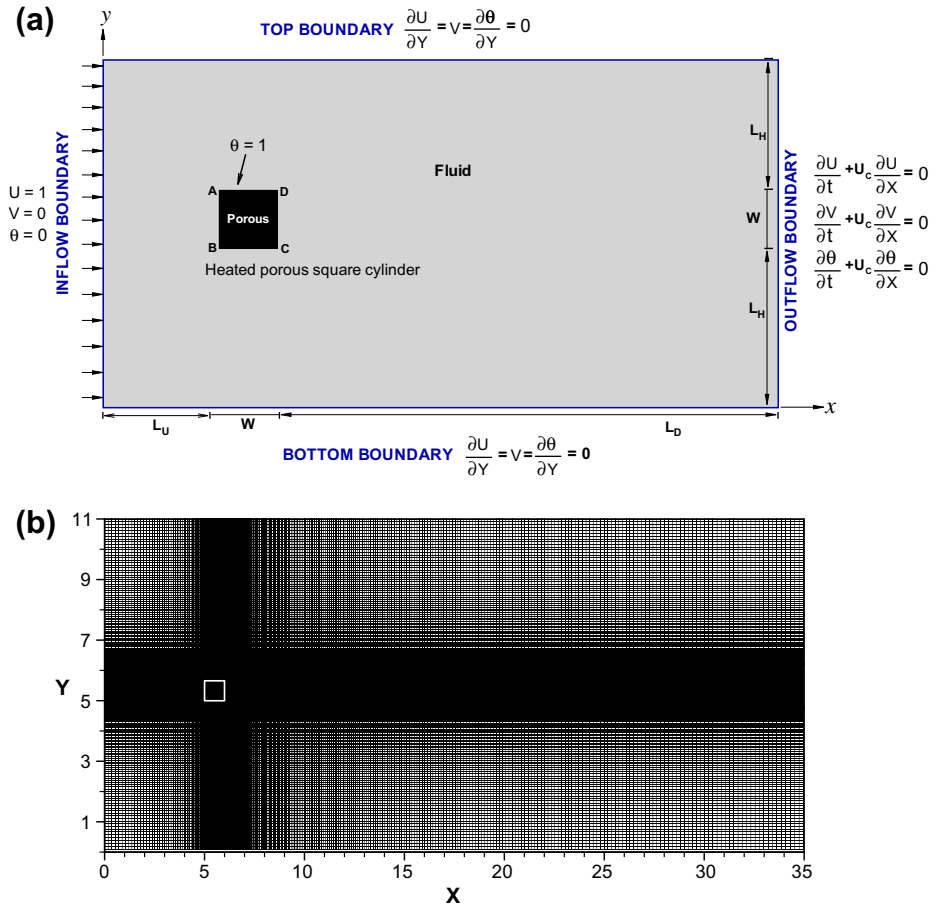

Fig. 1. (a) Schematic diagram of the computational set-up (along with the boundary conditions) for the unconfined flow and heat transfer from a permeable square cylinder; (b) non-uniform mesh distribution in the computational domain.

tivity of the fluid-saturated porous cylinder is equal to the thermal conductivity of the fluid.

With these assumptions, the hydrodynamic and energy equations can be readily developed as follows [15]:

Continuity equation:

$$\frac{\partial u}{\partial x}+\frac{\partial v}{\partial y}=0 \tag{1}$$

Momentum equations:

$$\rho\left(\frac{1}{\epsilon}\frac{\partial u}{\partial t}+\frac{u}{\epsilon^2}\frac{\partial u}{\partial x}+\frac{v}{\epsilon^2}\frac{\partial u}{\partial y}\right)=-\frac{\partial p}{\partial x}+\frac{\mu_e}{\epsilon}\left(\frac{\partial^2 u}{\partial x^2}+\frac{\partial^2 u}{\partial y^2}\right)-\frac{\mu}{\kappa}u-\frac{\rho F}{\sqrt{\kappa}}|\vec{V}|u \tag{2}$$

$$\rho\left(\frac{1}{\epsilon}\frac{\partial v}{\partial t}+\frac{u}{\epsilon^2}\frac{\partial v}{\partial x}+\frac{v}{\epsilon^2}\frac{\partial v}{\partial y}\right)=-\frac{\partial p}{\partial y}+\frac{\mu_e}{\epsilon}\left(\frac{\partial^2 v}{\partial x^2}+\frac{\partial^2 v}{\partial y^2}\right)-\frac{\mu}{\kappa}v-\frac{\rho F}{\sqrt{\kappa}}|\vec{V}|v \tag{3}$$

where $|\vec{V}|=\sqrt{u^2+v^2}, F=\frac{1.75}{\sqrt{150}}\frac{1}{\epsilon^{3/2}}$ is the inertial factor defined by Fu et al. [6].

Energy equation:

$$\rho C_p\frac{\partial T}{\partial t}+\frac{\rho C_p}{\epsilon}\left(u\frac{\partial T}{\partial x}+v\frac{\partial T}{\partial y}\right)=k_e\left(\frac{\partial^2 T}{\partial x^2}+\frac{\partial^2 T}{\partial y^2}\right) \tag{4}$$

The following characteristic scales are introduced to non-dimensionalized the above governing equations:

$$X=\frac{x}{W},\quad Y=\frac{y}{W},\quad \tau=\frac{tU_\infty}{W},\quad P=\frac{p}{\rho U_\infty^2},$$
$$U=\frac{u}{U_\infty},\quad V=\frac{u}{U_\infty},\quad \theta=\frac{(T-T_\infty)}{(T_w-T_\infty)}$$

The dimensionless form of the governing equations for the incompressible flow of a constant viscosity fluid past a porous square cylinder, written as a single set of equations, applicable for both the fluid and porous region is presented as follows:

$$\frac{\partial U}{\partial X}+\frac{\partial V}{\partial Y}=0 \tag{5}$$

$$\frac{\partial U}{\partial \tau}+\frac{1}{\epsilon}\left(U\frac{\partial U}{\partial X}+V\frac{\partial U}{\partial Y}\right)=-\epsilon\frac{\partial P}{\partial X}+\Lambda\frac{1}{Re}\left(\frac{\partial^2 U}{\partial X^2}+\frac{\partial^2 U}{\partial Y^2}\right)-C_1\epsilon\frac{1}{ReDa}U-C_2\frac{1.75}{\sqrt{150}}\frac{1}{\sqrt{Da}}\times\frac{\sqrt{U^2+V^2}}{\sqrt{\epsilon}}U \tag{6}$$

$$\frac{\partial V}{\partial \tau}+\frac{1}{\epsilon}\left(U\frac{\partial V}{\partial X}+V\frac{\partial V}{\partial Y}\right)=-\epsilon\frac{\partial P}{\partial Y}+\Lambda\frac{1}{Re}\left(\frac{\partial^2 V}{\partial X^2}+\frac{\partial^2 V}{\partial Y^2}\right)-C_1\epsilon\frac{1}{ReDa}V-C_2\frac{1.75}{\sqrt{150}}\frac{1}{\sqrt{Da}}\times\frac{\sqrt{U^2+V^2}}{\sqrt{\epsilon}}V \tag{7}$$

$$\frac{\partial\theta}{\partial\tau}+\frac{1}{\epsilon}\left(U\frac{\partial\theta}{\partial X}+V\frac{\partial\theta}{\partial Y}\right)=\frac{R_k}{Re.Pr}\left(\frac{\partial^2\theta}{\partial X^2}+\frac{\partial^2\theta}{\partial Y^2}\right) \tag{8}$$

here,

$$C_1, C_2 = \text{Binary constant}\begin{cases}0, & \text{outside the porous cylinder}\\ 1, & \text{inside the porous cylinder}\end{cases}$$

$$\epsilon = \text{Porosity}\begin{cases}1, & \text{outside the porous cylinder}\\ 0<\epsilon<1, & \text{inside the porous cylinder}\end{cases}$$

The dimensionless variables are defined as: $Re = \rho U_\infty W/\mu$ is the Reynolds number, $Pr = \mu\, C_p/k$ is the Prandtl number, $Da = \kappa/W^2$ is the Darcy number, ϵ is the porosity, $\Lambda = \mu_e/\mu$, denotes the viscosity ratio. and $R_k = k_e/k_f$ is the thermal conductivity ratio. The viscosity ratio and thermal conductivity ratio are assumed to be equal to unity in this study.

2.3. Boundary conditions

Inflow boundary (inlet): $U = 1$, $V = 0$ and $\theta = 0$.

Top and bottom boundaries: $\frac{\partial U}{\partial Y}=0$, $V = 0$ and $\frac{\partial\theta}{\partial Y}=0$.

Outflow boundary (exit): The convective boundary condition has been used as it decreases the number of time step, and allows lower downstream length (L_d) to be used [22], and is given by

$$\frac{\partial\phi}{\partial t}+U_c\frac{\partial\phi}{\partial X}=0 \tag{9}$$

where U_c is the average non-dimensional streamwise velocity (equal to unity) and ϕ is the dependent variable U, V or θ. For the temperature field, a constant temperature boundary condition is used on the surface of the porous cylinder. The cylinder exchanges heat with the cold fluid flowing through and around it, which is at a uniform temperature (T_∞) far away.

2.4. Governing parameters

The porosity (ϵ) and the Darcy number (Da) could be related through the Carman–Kozeny relation [17] given by

$$\kappa=\frac{1}{180}\frac{\epsilon^3 d_p^2}{(1-\epsilon)^2} \tag{10}$$

where, κ is the permeability and d_p is the characteristic diameter of a particle in the permeable cylinder, each of which may be of 100 μm in diameter [23].

The coefficient of the drag (C_D) on the cylinder is given by

$$C_D = C_{DP}+C_{DV}=\frac{F_D}{\frac{1}{2}\rho U_\infty^2} \tag{11}$$

where C_{DP} and C_{DV} represent the drag coefficient due to pressure and viscous force, respectively. F_D is drag force acting on the cylinder. The drag coefficients due to pressure and viscous forces can be obtained from the following expression:

$$C_{DP}=2.0\int_0^1 (P_f-P_r)dY,\quad C_{DV}=\frac{2.0}{Re}\int_0^1\left[\left(\frac{\partial U}{\partial Y}\right)_b+\left(\frac{\partial U}{\partial Y}\right)_t\right]dX$$

with P representing the non-dimensional pressure acting on the surface of the cylinder. The subscripts f, r, t and b refer to front, rear, top and bottom surface of the cylinders.

Heat transfer from the permeable cylinder to the flowing fluid is calculated from the local Nusselt number given by $Nu = -R_k\frac{\partial\theta}{\partial n}$. Here, n is the direction normal to a cylinder surface and R_k is the ratio of thermal conductivity of the porous material (k_e) and fluid (k_f). R_k is assumed to be equal to 1 in this study. Average heat transfer at any face of the cylinder is obtained by integrating the local Nusselt number along that face. The surface averaged Nusselt number on the front (f), rear (r), top (t) and bottom (b) face of the cylinder (see Fig. 1a) is calculated as

$$Nu_f=-\int_A^B Nu\,dY;\quad ssNu_t=-\int_D^A Nu\,dX;$$
$$Nu_r=-\int_C^D Nu\,dY \text{ and } Nu_b=-\int_B^C Nu\,dX. \tag{12}$$

The total heat transfer rate from the permeable cylinder is presented in terms of mean Nusselt number (Nu_M). Nu_M is obtained as a mean value of the average Nusselt number on all the surfaces as shown below

$$Nu_M=\frac{1}{4}\sum_{AB}Nu_{f,r,t,b}. \tag{13}$$

3. Numerical procedure and validation

3.1. Numerical method

The numerical simulation performed here is based on finite volume method. Staggered grid system is used where the velocity components are stored at cell faces while scalar quantities such as the pressure and temperature are stored at the cell center. The governing Eqs. (5)–(8) are solved numerically using SIMPLE [24] algorithm. For this purpose the governing equations are integrated over each control volume to obtain a set of linear algebraic equations. We used a first order implicit scheme to discretize the time derivatives and a third-order accurate QUICK scheme (Quadratic Upwind Interpolation for Convective Kinematics) [25] for the convective terms. The diffusion terms are discretized by central difference scheme. The pressure link between continuity and momentum is accomplished by transforming the continuity equation into a Poisson equation for pressure. The Poisson equation implements a pressure correction for a divergent velocity field. At each time step the resulting tridiagonal system of algebraic equations are solved through a block elimination method. Iterations are continued until a divergence-free velocity field is obtained. Convergence is assumed to be achieved when the summation of residuals decreased to $\leqslant 10^{-6}$ for all equations.

3.2. Grid structure

At the interface between the fluid and the porous layers, porosity (ϵ) and permeability (Da) usually undergo a large change. In order to handle the abrupt change in the these parameters, the harmonic-mean formulation, suggested by Patankar [24], is used. Besides, a finer grid is also imposed near the porous-fluid interface. A non-uniform grid distribution is used in this study. Grids are stretched through an arithmetic progression. The minimum distance of the first grid point from the fluid porous interface is $\delta = 0.001$. At a sufficient far distance, a uniform grid is used with grid size ($\Lambda = 0.2$). A grid sensitivity study is made at $Re = 40$, $Da = 10^{-6}$ to check the dependence of flow and heat transfer parameters such as C_D and Nu on the grid size and the downstream length (L_d). A series of test runs were made for determining the optimal grid size and the runs were performed with various grid sizes for three different downstream length viz., $L_d = 25$, 35 and 45.

The code is tested for four different grid sizes namely 225×125, 450×250, 675×375 and 900×500 (also called as Grid A, Grid B, Grid C and Grid D, respectively) at $Da = 10^{-6}$, with the first and second number being the number of mesh points in the x and y direction. Table 1 summarizes the effect of various grid size and downstream length (L_d) on the computed drag coefficient and Nusselt number. Our grid sensitivity study suggests that grid

Table 1
Grid sensitivity and downstream length dependence test on drag coefficient (C_D) and mean Nusselt number (Nu_M) at $Da = 10^{-6}$ and $Re = 40$.

Grids ($m \times n$)	Drag coefficient (C_D)			Nusselt number (Nu)		
	$L_d = 25$	$L_d = 35$	$L_d = 45$	$L_d = 25$	$L_d = 35$	$L_d = 45$
225×125 (Grid A)	1.952	1.916	1.916	2.428	2.501	2.501
450×250 (Grid B)	1.798	1.793	1.792	2.666	2.668	2.668
675×375 (Grid C)	1.763	1.760	1.760	2.652	2.670	2.670
900×500 (Grid D)	1.761	1.758	1.759	2.650	2.678	2.679

Table 2
Comparison of drag coefficient (C_D) and recirculation length (L_r) for different Re and $Pr = 0.7$ with the literature for the case of a solid square cylinder in an unbounded flow domain.

Re	Drag coefficient (C_D)					Wake length (L_r)			
	a[a]	b[b]	c[c]	d[d]	Error (%)	a[a]	c[c]	d[d]	Error (%)
1	14.376	–	–	14.400[e]	0.167	–	–	–	–
5	5.007	–	4.814	4.840[e]	3.335	0.313	0.30	0.309[e]	1.278
10	3.375	–	–	3.390[e]	0.444	0.645	–	0.650[e]	0.775
20	2.402	–	–	2.401[e]	0.004	1.300	–	1.390[e]	6.923
30	2.014	–	–	2.010[e]	0.199	1.985	–	2.110[e]	6.290
40	1.798	1.980	1.899	1.767[e]	1.724	2.665	2.700[e]	2.822	1.313

[a] Present study.
[b] Franke et al. [1].
[c] Paliwal et al. [26].
[d] Sharma and Eswaran [4].
[e] Data used for the calculation of percentage error.

Table 3
Comparison of mean Nusselt number (Nu_M) at $Pr = 0.71$ and $Pr = 10$ with the literature for the case of a solid square cylinder in an unbounded flow domain.

Re	Nusselt number (Nu)						
	$Pr = 0.7$			$Pr = 10$			
	a[a]	d[d]	Error (%)	a[a]	b[b]	c[c]	Error (%)
1	0.674	0.650	3.560	1.572	–	1.569[e]	0.191
5	1.187	1.200	1.095	2.686	–	2.706[e]	0.745
10	1.541	1.580	2.530	3.491	–	3.530[e]	1.117
20	2.124	2.190	3.107	4.752	–	4.824[e]	1.515
30	2.378	2.390	0.504	5.798	–	5.805[e]	0.121
40	2.666	2.620	1.725	6.520	6.908	6.574[e]	0.828

[a] Present study.
[b] Paliwal et al. [26].
[c] Dhiman et al. [5].
[d] Sharma and Eswaran [4].
[e] Data used for the calculation of percentage error.

Table 5
Comparison of overall wake length (L_r) behind the an unbounded permeable square cylinder in uniform flow at different Darcy numbers (Da) and Porosity ($\epsilon = 0.7$) with those of Yu et al. [14].

Da	Wake length (L_r)	
	a[a]	b[b]
5×10^{-3}	0.872	0.869
2×10^{-3}	1.051	1.042
1×10^{-3}	1.182	1.175
1×10^{-4}	1.265	1.258
1×10^{-5}	1.292	1.292
5×10^{-6}	1.295	1.293
1×10^{-6}	1.300	1.300

[a] Wu and Wang [15].
[b] Present study.

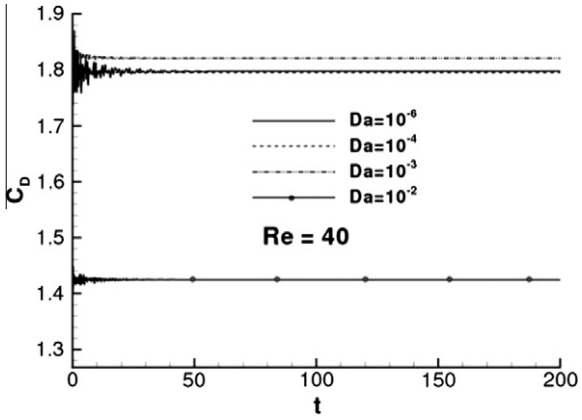

Fig. 2. Time evolution of drag coefficient (C_D) at different Darcy numbers ($Da = 10^{-6}$, 10^{-4}, 10^{-3} and 10^{-2}) at $Re = 40$, for the flow through and around a permeable square cylinder.

independent results could be achieved using Grid B at $L_d = 35$. The mesh distribution in the computational domain with Grid B is shown in Fig. 1b.

3.3. Code validation

The best way of verifying the code for the flow past a permeable body is to set the Darcy number and porosity to very low values and check if it reproduces the results for the flow past a corresponding solid body (in this case, a solid square cylinder in an unbounded domain). For this purpose we used very small values of Darcy number ($Da = 10^{-15}$) and porosity ($\epsilon = 0.1$) in Eqs. (6)–(8)

Table 4
Comparison of mean Nusselt number (Nu_M) along the bottom surface of a permeable square cylinder confined by a channel at $Re = 100$ for different Darcy numbers (Da) and Porosity (ϵ) with those of Wu and Wang [15].

Da	Nusselt number (Nu_M)								
	$\epsilon = 0.4$			$\epsilon = 0.6$			$\epsilon = 0.8$		
	a[a]	b[b]	Error (%)	a[a]	b[b]	Error (%)	a[a]	b[b]	Error (%)
10^{-2}	17.04	16.73	1.85	17.22	16.88	2.01	17.37	16.99	2.23
10^{-3}	16.58	16.37	1.28	16.34	16.05	1.81	16.20	15.98	1.38
10^{-4}	15.91	15.75	1.02	15.82	15.59	1.48	15.79	15.61	1.15
10^{-5}	15.66	15.55	0.71	15.66	15.52	0.90	15.68	15.57	0.71
10^{-6}	15.62	15.53	0.58	15.64	15.47	1.10	15.66	15.53	0.83
Impermeable cylinder	15.61	15.50	0.71	15.61	15.50	0.71	15.61	15.50	0.71

[a] Present study.
[b] Wu and Wang [15].

for the porous region to compute flow and thermal field. Our computed results for the drag coefficient (C_D), wake length (L_r) of the permeable square cylinder, at these values of *Da* and ϵ compared well with the results obtained for the case of a solid square cylinder and with the published numerical results of Franke et al. [1], Paliwal et al. [26], Sharma and Eswaran [4] and Dhiman et al. [5] (see Table 2). Thus, we find the porous cylinder, essentially, behaves as an impermeable cylinder for the above mentioned values of *Da* and ϵ. The computed Nusselt number (Nu_M) for the case of a permeable cylinder (for the above mentioned values of *Da* and

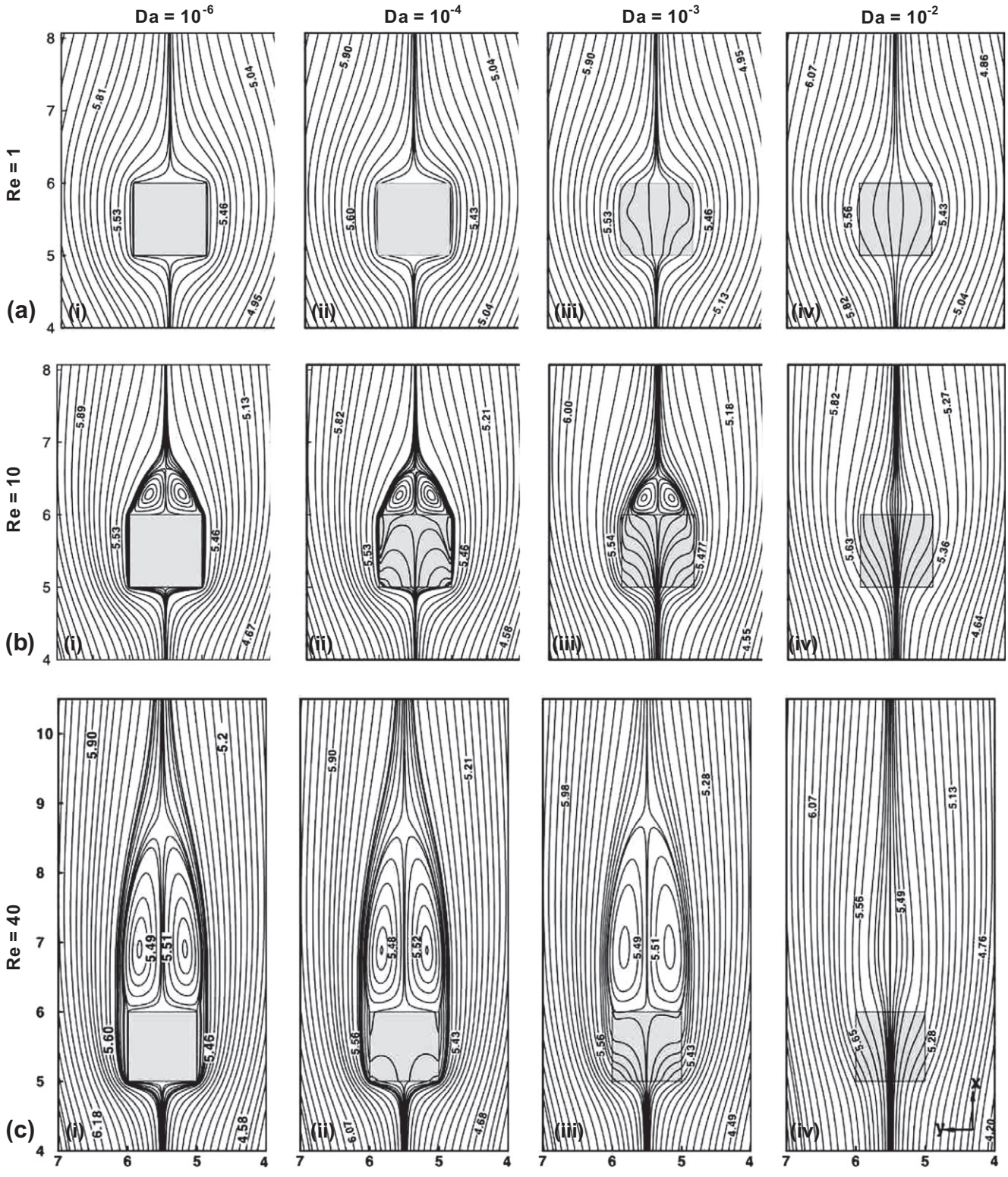

Fig. 3. Streamlines through and around the permeable square cylinder at different Reynolds numbers and Darcy numbers: (a) *Re* = 1; (b) *Re* = 10 and (c) *Re* = 40.

ϵ) and solid cylinder are found to be in good agreement with the findings of Sharma and Eswaran [4] at $Pr = 0.71$ and for $Pr = 10$ and with those of Paliwal et al. [26] as seen in Table 3. The present code has been further validated with the numerical results of Wu and Wang [15] for the mean Nusselt number at the bottom surface of a porous square cylinder, placed symmetrically in a channel, at $Re = 100$ for various Da and ϵ. The compared results are well within an error of 2.5% as presented in Table 4. To further validate the correctness of our code we compared the wake length behind the porous square cylinder in an unbounded domain at $Re = 20$ for various Darcy numbers with those of Yu et al. [14], shown in Table 5, which is in excellent agreement.

4. Results and discussion

4.1. Flow characteristics

4.1.1. Parameters used in the study

In the present study, the following values for the flow and heat transfer parameters are considered:

Reynolds number: $Re = 1$, 2 and 5–40 in steps of 5 .
Darcy number: $Da = 10^{-6}$, 10^{-4}, 10^{-3} and 10^{-2}.
Porosity: $\epsilon = 0.629$, 0.8, 0.977, 0.993.
Prandtl number: $Pr = 0.71$ (air).

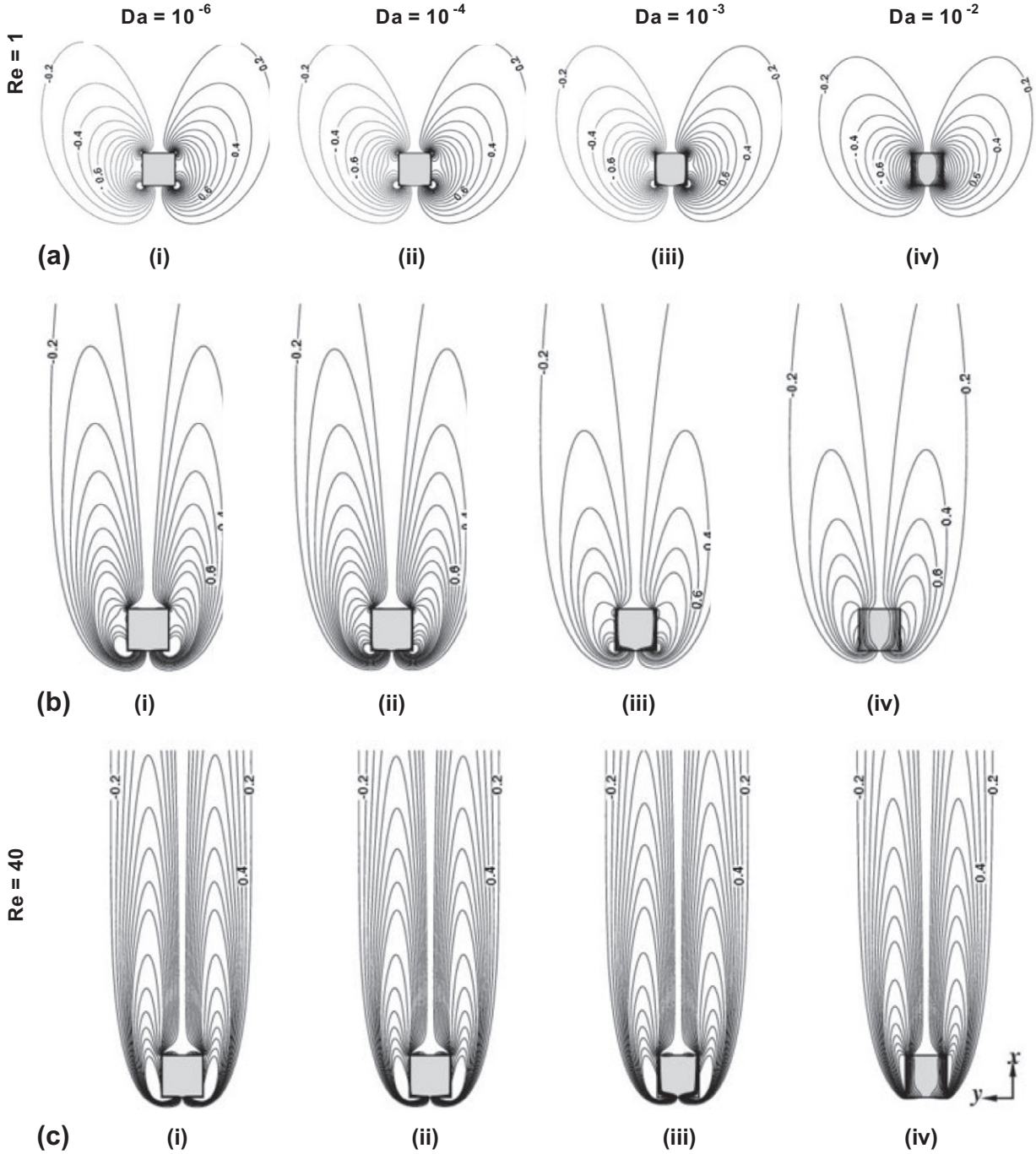

Fig. 4. Vorticity contours for the flow through and around a permeable square cylinder at different Reynolds numbers and Darcy numbers: (a) $Re = 1$; (b) $Re = 10$ and (c) $Re = 40$.

4.1.2. Time evolution of drag coefficient

The time evolution of drag coefficient is shown in Fig. 2 at $Da = 10^{-6}$, $Da = 10^{-4}$, $Da = 10^{-3}$ and $Da = 10^{-2}$, at $Re = 40$. The flow becomes steady after an initial transition for all Darcy numbers considered in this study.

4.1.3. Streamline pattern

The flow pattern of a impermeable cylinder is well known. The flow is fully attached at $Re = 1$. The flow separates at the trailing edge of the cylinder (at $Re = 2$), reattaches at the wake center line and then forms a recirculating eddy [4]. For a permeable cylinder the case is entirely different. A permeable cylinder allows a finite amount of fluid to pass through it. The amount of fluid penetrating the surface depends on the permeability of the material of the cylinder. Low permeability means more obstruction to fluid flow. In Fig. 3a–c we present the streamlines for Reynolds numbers 1, 10 and 40 at Darcy numbers 10^{-6}, 10^{-4}, 10^{-3} and 10^{-2}. At $Da = 10^{-6}$ for all Re presented here, the streamline does not pass through the cylinder and the streamline pattern appears very similar to an impermeable cylinder. Thus, it can be concluded that a permeable cylinder behaves more or less like a solid cylinder at $Da = 10^{-6}$. Upon increasing the Darcy number, for example, at $Da = 10^{-4}$ (see Fig. 3a(ii), b(ii) and c(ii)) the streamlines penetrating through the cylinder are clearly evident (for $Re > 1$). The fluid enters the cylinder (through the front face) and takes a curved path through the cylinder. With increase in permeability, the streamlines more easily penetrate the cylinder and the curvature of the streamlines keep decreasing with increase in Da. At the largest Da of 10^{-2} considered here, almost all the streamlines pass through the cylinder and are more elongated.

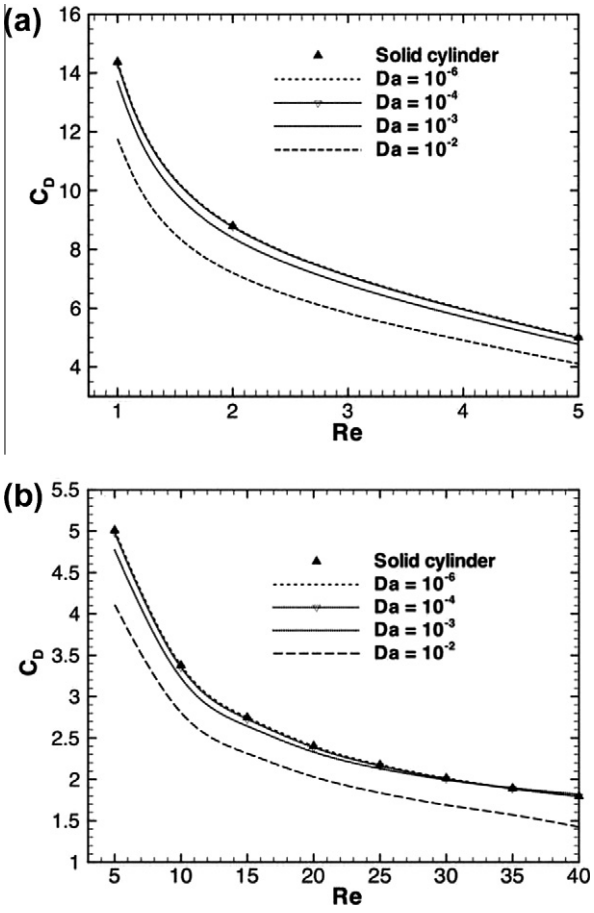

Fig. 5. Drag coefficient (C_D) at $Da = 10^{-6}$, 10^{-4}, 10^{-3} and 10^{-2} as a function of Reynolds numbers for the flow through and around a permeable square cylinder: (a) $1 \leqslant Re \leqslant 5$; (b) $5 \leqslant Re \leqslant 40$. Results are also included for the case of solid square cylinder.

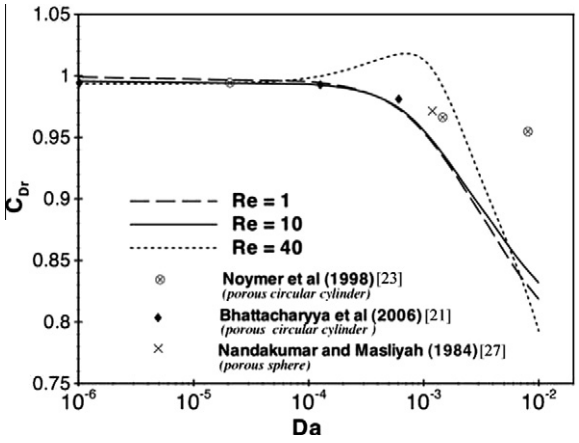

Fig. 6. Drag ratio (C_{Dr}) as a function of Da at $Re = 1$, 10 and 40. (See above-mentioned references for further information).

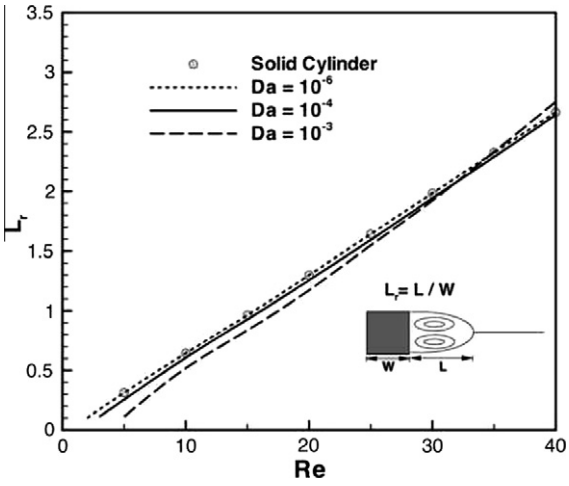

Fig. 7. Wake length (L_r) as a function Reynolds number for various Darcy numbers.

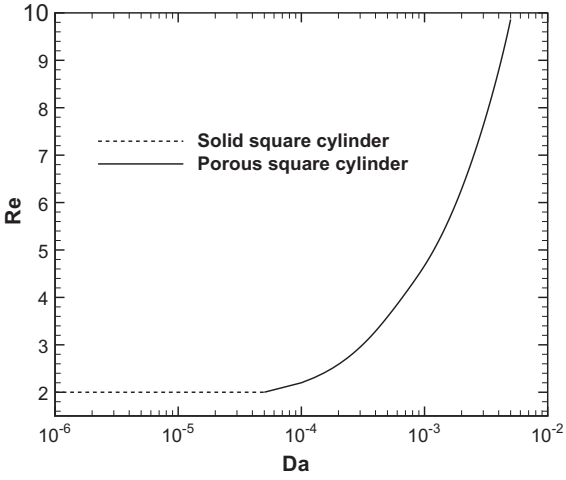

Fig. 8. Onset of flow separation at different Da.

4.1.4. Vorticity pattern

The vorticity contours are presented in Fig. 4a–c for Reynolds numbers 1, 10 and 40 for different Darcy numbers. Looking at Fig. 4 we find the vorticity is symmetric along a vertical centre line. At $Da = 10^{-6}$, the vortices are attached to the surface of the cylinder. With increasing *Da* the vortices slowly diffuse into the cylinder. At large Darcy number ($Da = 10^{-2}$) the vortices diffuse more easily into the cylinder as the cylinder allows a large amount of fluid to pass through it. Referring to Fig. 4a(i and iv) we see that the size of the vortex is smaller at large *Da* compared to small *Da* values. This is due to a decrease in strength of the vortices with increase in *Da*. At higher Reynolds numbers (*Re* = 10 and 40), the vor-

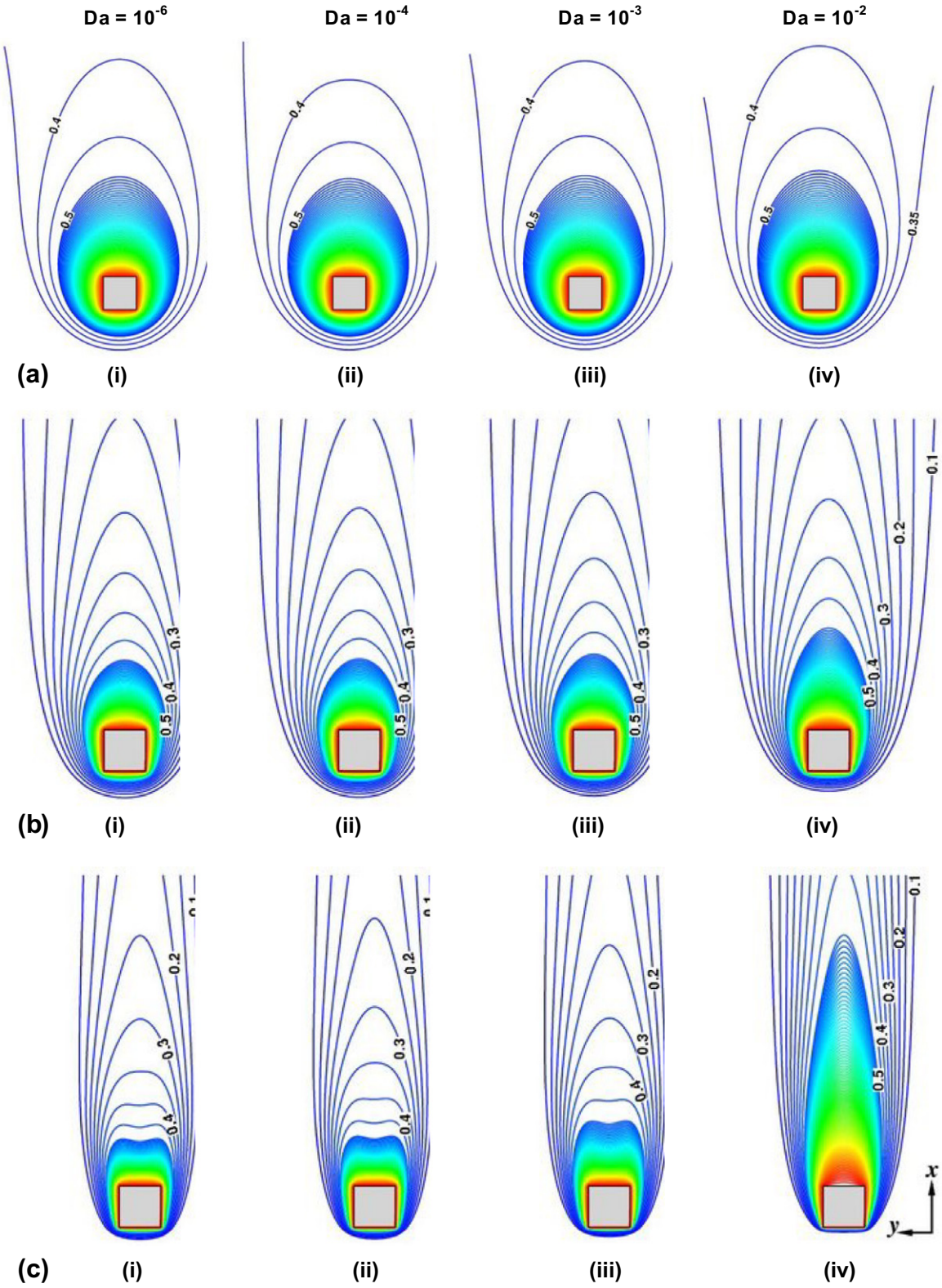

Fig. 9. Isotherms around the permeable square cylinder at different Reynolds numbers and Darcy numbers: (a) *Re* = 1; (b) *Re* = 10 and (c) *Re* = 40.

tices are more elongated and are advected along the flow. Two secondary vortices appear behind the cylinder at $Da = 10^{-6}$. These secondary vortices disappear for $Da \geqslant 10^{-3}$ at $Re = 10$ and at $Da = 10^{-2}$ for $Re = 40$. The shear layers formed along the cylinder surface become more and more narrower with increasing Da as their strength reduce.

4.1.5. Drag coefficient

The coefficient of drag experienced by the permeable cylinder, calculated as per Eq. (11), is presented in Fig. 5a and b for $1 \leqslant Re \leqslant 5$ and $5 \leqslant Re \leqslant 40$ for various Da. In order to compare the drag of the permeable cylinder with that of impermeable cylinder, the C_D of the latter is also plotted. From the figure, we observe that the drag coefficient of the permeable cylinder at low $Da(=10^{-6})$ coincides with that of impermeable cylinder and decreases with increase in Da. A highly permeable cylinder ($Da = 10^{-2}$) allows a finite amount of fluid to pass through itself (as can be see in the streamline plots) offering less resistance to fluid flow. Whereas, at low permeability values, the cylinder obstructs the fluid passing through it and behaves more of a bluff body. Hence, at any Reynolds number, C_D increase with decrement in Da. Having a close look at Fig. 5a, one could find that the C_D vs. Re profile at $Da = 10^{-3}$ shows a different behaviour compared to other Da values. The coefficient of drag at $Da = 10^{-3}$ remains less than the C_D of impermeable cylinder as well as porous cylinder at $Da = 10^{-6}$ and 10^{-4} for $Re \leqslant 25$ and it approaches the value of impermeable cylinder for $Re > 25$ meeting the curve for a impermeable cylinder at $Re = 37$ before finally reaching a value slightly higher than the impermeable cylinder at $Re = 40$. This kind of behaviour has also been predicted by Noymer et al. [23] for the case of a permeable circular cylinder. In their study C_D of the permeable cylinder was found to be higher than the corresponding impermeable cylinder in the range $5 \times 10^{-5} < Da < 10^{-2}$ at $Re = 100$.

4.1.6. Drag ratio

The drag coefficient of the permeable cylinder normalized by the corresponding drag coefficient of impermeable cylinder and defined as drag ratio (C_{Dr}) is presented in Fig. 6 for $Re = 1$, 10 and 40 as a function of Da. From the figure we find that C_{Dr} remain close to unity in the range $10^{-6} \leqslant Da \leqslant 10^{-4}$ and it decreases rapidly beyond this range for $Re = 1$ and 10. Ironically, at $Re = 40$, this is not the case; C_{Dr} remains close to unity for $Da < 2 \times 10^{-5}$ and increases beyond this to reach a peak value of 1.013 (1.3% increase in drag coefficient compared to impermeable cylinder) at $Da = 7 \times 10^{-4}$ and then drops rapidly. A similar trend was observed by Noymer et al. [23] in their computational and experimental study of flow past a permeable circular cylinder at $Re = 100$ and 1000.

4.1.7. Wake length

For the flow past a solid square cylinder, the flow separates from a large section of the body surface thus creating a significant wake downstream. Two counter rotating eddies are formed behind the cylinder. These eddies are symmetric in shape and grow in size with increase in Re. For the case of permeable square cylinder, too, we find two counter rotating eddies behind the cylinder that depends on Da and Re. We define the length of the recirculation region as the stream-wise distance from the rear surface of the cylinder to the re-attachment point along the wake centerline (L_r). The variation of L_r behind the permeable square cylinder with Reynolds number is shown in Fig. 7 at $Da = 10^{-6}$, 10^{-4} and 10^{-3}. L_r at $Da = 10^{-6}$ almost coincides with that of impermeable cylinder as the cylinder is impermeable for fluid flow and hence behaves as a solid cylinder for all Re. Whereas, a higher Da of 10^{-4} we find a monotonous decreases in L_r for all Re. However, at Da of 10^{-3}, there is a non-monotonous trend of L_r, i.e., it decreases for $5 \leqslant Re < 35$ and increases for $Re > 35$. Thus, at $Re = 40$ and $Da = 10^{-3}$ we find a larger wake length compared to the lower values of Da as is evident from the streamline contour in Fig. 3c(iii). At $Da = 10^{-2}$, the recirculating eddy vanishes as most of the fluid enters the cylinder and exits at the rear face.

4.1.8. Flow Separation

Fig. 8 illustrates the Reynolds number at which flow separation occurs at different Darcy numbers. Similar to the case of a solid cylinder where flow separation from the cylinder occurs at $Re \geqslant 2$, flow separation for a permeable cylinder occurs at $Re \geqslant 2$ for Darcy numbers in the range $10^{-6} \leqslant Da \leqslant 10^{-4}$. Beyond $Da = 10^{-4}$, the Reynolds number at which flow separation occurs is delayed. For example, flow separation occurs at $Re = 2.5$ for $Da = 10^{-4}$ and at $Re = 5$ for $Da = 10^{-3}$. Hence, for a permeable cylinder the flow separation is delayed that depends on Da and Re.

4.2. Heat transfer characteristics

4.2.1. Isotherms

Typical isotherm profiles around the permeable square cylinder at $Re = 1$, 10 and 40 are presented in Fig. 9a–c at the same instant of time for which the streamlines have been shown in Fig. 3a–c. The size of the thermal plume increases with increase in Da for a fixed Re. At $Re = 1$, there is no significant difference in the size of the thermal plume with increase in Da. Upon increasing the Reynolds

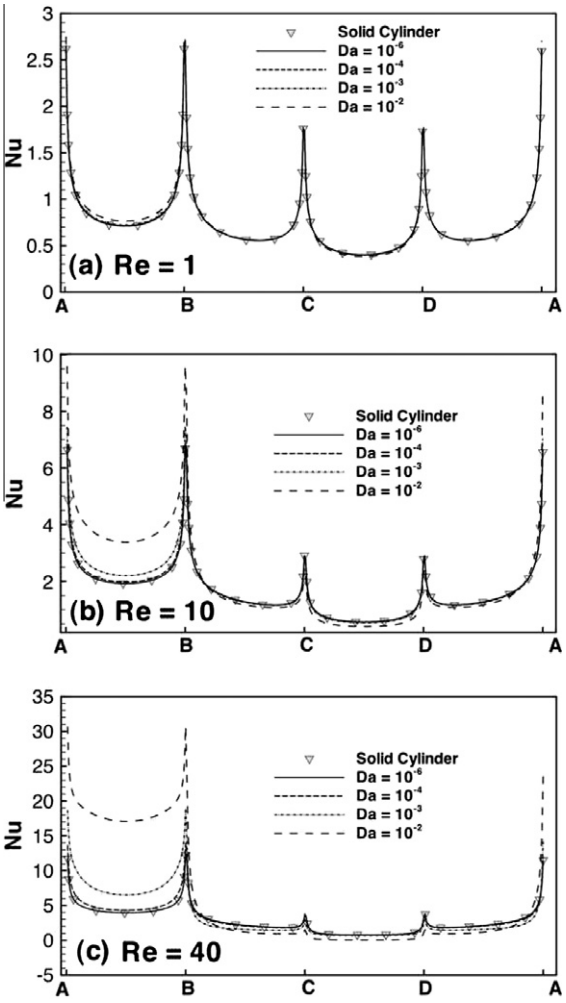

Fig. 10. Local Nusselt number (Nu) distribution along the surface of the permeable cylinder for various Darcy numbers at (a) $Re = 1$, (b) $Re = 10$ and (c) $Re = 40$. Data for solid square cylinder is also shown.

number, the plume increases in size with increase in *Da*. For example, at *Re* = 40, comparing Fig. 9a–c we find that the size of the thermal plume is the largest at $Da = 10^{-2}$ while it is the shortest at $Da = 10^{-6}$. At low *Da*, the fluid passing through the cylinder is negligible. As more and more fluid penetrate the cylinder, they carry away more heat with them and hence we find a long thermal plume at high *Da* compared to lower *Da* case. For all *Da* and *Re* considered here, the isotherms shows a steady thermal plume behind the cylinder in the streamwise direction.

4.2.2. Local Nusselt number along the surface

The variation of local Nusselt number (*Nu*) along the surface of the permeable cylinder is shown in Fig. 10a–c for *Re* = 1, 10 and 40 at $Da = 10^{-6}$, 10^{-4}, 10^{-3},10^{-2} and for solid cylinder as well. In general, the local Nusselt number distribution shows high values of *Nu* at the corners (A–D) of the cylinder due to large temperature gradient at the surface. The local Nusselt number at each corner and at all surface of the permeable cylinder increases with increase in *Re*. Highest *Nu* occurs at the front face corners (A and B) of the cylinder due maximum crowding of isotherms at this face. There is a local minimum at the center of the rear face (CD) at all Re. At $Da = 10^{-6}$, *Nu* along the surface coincides with that of solid cylinder at all *Re*. At *Re* = 1, there is not any significant change in the *Nu* with the variation of *Da* from 10^{-6} to 10^{-4} at any face. At $Da = 10^{-2}$, *Nu* along the front face has slightly increased while it slightly decreases along the rear face. At *Re* = 40, increasing *Nu* with increase in *Da* is observed along the front face (AB) and decreasing *Nu* at the remaining faces. This is due to clustering and spreading out of the isotherms along the front and rear face, respectively, as is evident in Fig. 9c(i and iv), when *Da* is varied from 10^{-6} to 10^{-2}.

4.2.3. Average Nusselt number along the faces

Fig. 11a–c show the representative variation of the average Nusselt number at each of the face of the permeable cylinder as a function of Reynolds number at different Darcy numbers. In general, the front face has the highest average Nusselt number, since the incoming fluid is in direct contact with this surface followed by the top/bottom face and the rear face. The average Nusselt number along the faces shows a strong dependence on *Da*. This dependence is more prominent for *Re* > 5. At small values of Darcy numbers ($Da = 10^{-6}$) the average Nusselt number along the faces are almost the same as that of impermeable cylinder for the range of Reynolds numbers considered here. For a fixed *Re*, when *Da* is varied from 10^{-6} to 10^{-2}, Nu_f increases while Nu_r, Nu_t and Nu_b decrease.

4.2.4. Mean Nusselt number

The variation of mean Nusselt number of the cylinder is illustrated in Fig. 11d as a function of Reynolds number for $Da = 10^{-6}$, 10^{-4}, 10^{-3} and 10^{-2}. For comparison, the mean Nusselt number of solid cylinder is also included. From this plot, we observe that the heat transfer rate increases almost linearly with increase in

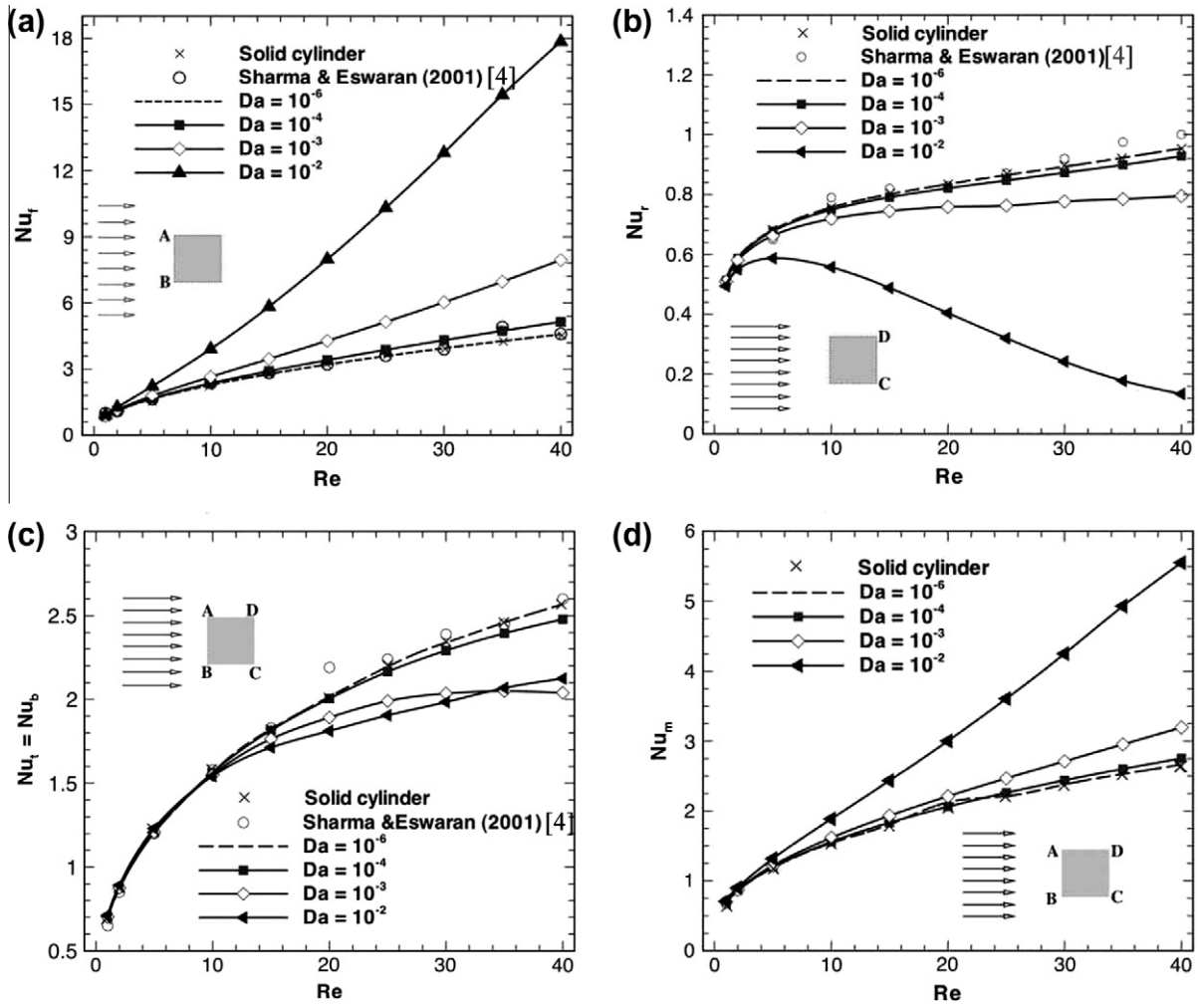

Fig. 11. Effect of Darcy number on local Nusselt number at different Reynolds number on (a) Front (b) top and bottom (c) rear face of the heated permeable square cylinder in an unbounded domain. The mean Nussult number (Nu_M) is shown in figure (d). Subscripts: *f*, front; *t*, top; *b*, bottom ; *r*, rear and *M*, mean.

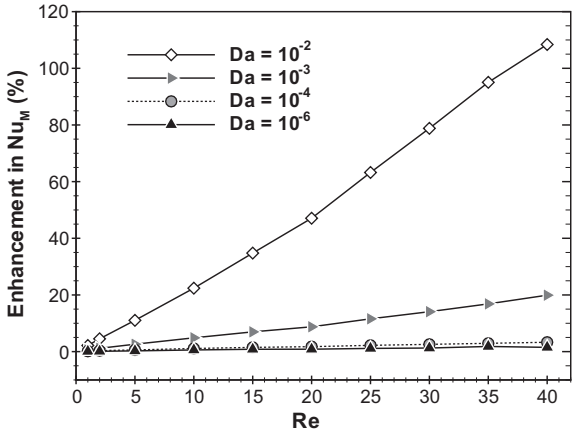

Fig. 12. Percentage increase in mean Nusselt number (Nu_M) of the porous square cylinder as a function of Reynolds number for various Darcy numbers.

Re for any *Da*. Nu_M at $Da = 10^{-6}$ coincides with that of solid cylinder. With increasing Darcy number one can find that there is a considerable amount of augmentation in heat transfer rates. Heat transfer augmentation is more prominent at higher *Re* compared to low *Re*. For example, percentage increase in Nu_M at $Re = 1$ at $Da = 10^{-4}$, 10^{-3} and 10^{-2} is 0.15%, 0.58% and 2.16%, respectively, compared to that of a solid cylinder. Whereas, this percentage increased to 3.31%, 19.91% and 108.4% for the same values of *Da* at $Re = 40$ as seen in Fig. 12.

5. Conclusion

The flow and heat transfer characteristics of a permeable square cylinder placed in a uniform flow and maintained at a constant temperature has been studied using Brinkman model. The effect of permeability on the flow and thermal pattern has been studied for various Reynolds. The major results of the study can be highlighted as follows:

1. The flow and thermal field remains steady for the range of Reynolds numbers and Darcy numbers considered in this study. The streamlines and isotherms are similar to that of a solid square cylinder at $Da = 10^{-6}$. With increase in Darcy number, i.e., $Da > 10^{-6}$, the streamlines show a different pattern with the lines partly passing through and partly around the cylinder. At high $Da(=10^{-2})$, almost all the streamlines pass through the cylinder resulting in a near-through flow. Vortex diffusion into the cylinder occurs with increasing *Da*. Flow separation is delayed for a permeable cylinder compared to the impermeable case.
2. The drag coefficient of the porous cylinder decreases with increase in Reynolds number and Darcy number. The porous cylinder allows a finite amount of fluid to pass through it. This results in a net decrease in resistance to flow and hence a decrease in drag coefficient.
3. The drag ratio of the porous cylinder decreases with increase in Darcy number for all Reynolds number and Darcy numbers except at $Re = 40$, where it increases at $Da = 8 \times 10^{-4}$ reaches a peak value and then starts decreasing.
4. The mean Nusselt number gradually increases with increase in Reynolds number and Darcy number. At low Darcy number $(=10^{-6})$, it approaches the value of an impermeable cylinder. A considerable amount of heat transfer augmentation occurs when the cylinder is permeable, that depends on *Re* and *Da*, compared to a solid cylinder.

Acknowledgements

I dedicate this paper to my beloved father M. Shanmugam (1948–2008) – S. Dhinakaran. The authors would like to thank the three anonymous reviewers for their constructive and valuable suggestion that helped us improve the quality of this paper.

References

[1] Franke R, Rodi W, Schonung B. Numerical calculation of laminar vortex shedding flow past cylinders. J Wind Eng Ind Aerodynam 1990;35:237–57.
[2] Zaki TG, Sen M, Gad-El-Hak M. Numerical and experimental investigation of flow past a freely rotational square cylinder. J Fluids Struct 1994;8:555–82.
[3] Sohankar A, Davidson L, Norberg C. Numerical simulation of unsteady flow around a square two-dimensional cylinder. In: Proc 12th Australian fluid mechanics conf; 1995. p. 517–20.
[4] Sharma A, Eswaran V. Heat and fluid flow across a square cylinder in the two-dimensional laminar flow regime. Numer Heat Transfer Part A 2004;45:247–69.
[5] Dhiman AK, Chabbra RP, Sharma A, Eswaran V. Effect of Reynolds number and Prandtl number on the heat transfer and fluid flow across a square cylinder in the steady flow regime. Numer Heat Transfer Part A 2007;49(7):717–31.
[6] Fu W, Huang H, Liou W. Thermal enhancement in laminar channel flow with a porous block. Int J Heat Mass Transfer 1996;39(10):2165–75.
[7] Guerroudj N, Kahalerras H. Mixed convection in a channel provided with heated porous blocks of various shapes. Energy Convers Manage 2010;51(3):505–17.
[8] Targui N, Kahalerras H. Analysis of fluid flow and heat transfer in a double pipe heat exchanger with porous structures. Energy Convers Manage 2008;49(11):3217–29 [Special issue 3rd international conference on thermal engineering: theory and applications].
[9] Abu-Hijleh BA. Heat transfer from a 2D backward facing step with isotropic porous floor segments. Int J Heat Mass Transfer 2000;43(15):2727–37.
[10] Jue T. Numerical analysis of vortex shedding behind a porous square cylinder. Int J Numer Methods Heat Fluid Flow 2004;14(5):649–63.
[11] Chen X, Yu P, Winoto S, Low H. Numerical analysis for the flow past a porous square cylinder based on the stress-jump interfacial-conditions. Int J Numer Methods Heat Fluid Flow 2008;18(5):635–55.
[12] Ochoa-Tapia JA, Whitaker S. Momentum transfer at the boundary between a porous medium and a homogeneous fluid – I. Theoretical development. Int J Heat Mass Transfer 1995;38(14):2635–46.
[13] Banu V, Narasimhan V. Investigation of vortex shedding behind a porous square cylinder using lattice Boltzmann method. Phys Fluids 2010;22:053605.
[14] Yu P, Zeng Y, Lee T, Bai H, Low H. Wake structure for flow past and through a porous square cylinder. Int J Heat Fluid Flow 2010;31:141–53.
[15] Wu H, Wang R. Convective heat transfer over a heated square porous cylinder in a channel. Int J Heat Mass Transfer 2010;53:1927–37.
[16] Wu H, Wang R. mixed convective heat transfer past a heated square porous cylinder in a horizontal channel with varying channel height. J Heat Transfer 2011;133:022503.
[17] Nield DA, Bejan A. Convection in porous media. New York: Springer Verlag; 1998.
[18] Whitaker S. The method of volume averaging. Dordrecht: Kluwer; 1999.
[19] Brinkman HC. A calculation of the viscous forced exerted by a flowing fluid on a dense swarm of particles. Appl Sci Res 1947;1:27–34.
[20] Brinkman HC. On the permeability of media consisting of closely packed porous particles. Appl Sci Res 1947;1:81–6.
[21] Bhattacharyya S, Dhinakaran S, Khalili A. Fluid motion through and around a porous cylinder. Chem Eng Sci 2006;61:4451–61.
[22] Sohankar A, Norberg C, Davidson L. Low-Reynolds number flow around a square cylinder at incidence: study of blockage, onset of vortex shedding and outlet boundary condition. Int J Numer Methods Fluids 1998;26:39–56.
[23] Noymer PD, Glicksman LR, Devendran A. Drag on a permeable cylinder in steady flow at moderate Reynolds number. Chem Eng Sci 1998;53(16):2859–69.
[24] Patankar SV. Numerical heat transfer and fluid flow. New York: Hemisphere Publishing Corporation, Taylor and Francis Group; 1980.
[25] Leonard BP. A stable and accurate convective modeling procedure based on quadratic upstream interpolation. Comput Methods Appl Mech Eng 1979;19:59–98.
[26] Paliwal B, Sharma A, Chhabra RP, Eswaran V. Power law fluid flow past a square cylinder: momentum and heat transfer characteristics. Chem Eng Sci 2003;58:5315–29.
[27] Nandakumar K, Masliyah JH. Laminar flow past a permeable sphere. Can J Chem Eng 1982;60:202–11.